



Published in final edited form as:

J Mater Chem B Mater Biol Med. 2017 August 14; 5(30): 6049–6057. doi:10.1039/C7TB01370A.

Co-delivery of paclitaxel and cisplatin with biocompatible PLGA-PEG nanoparticles enhances chemoradiotherapy in non-small cell lung cancer models

Jing Tian^{a,b,c,†}, Yuanzeng Min^{b,c,†}, Zachary Rodgers^{b,d}, Kin Man Au^{b,c}, C. Tilden Hagan IV^{b,e}, Maofan Zhang^{b,c,f}, Kyle Roche^{b,c}, Feifei Yang^{b,c,g}, Kyle Wagner^{b,c}, and Andrew Z. Wang^{b,c,*}

^aSchool of Biological and Environmental Engineering, Tianjin Vocational Institute, Tianjin 300410, P. R. China

^bLaboratory of Nano- and Translational Medicine, Lineberger Comprehensive Cancer Center, Carolina Center for Cancer Nanotechnology Excellence, Carolina Institute of Nanomedicine, University of North Carolina at Chapel Hill, Chapel Hill, NC 27599, USA

^cDepartment of Radiation Oncology, Lineberger Comprehensive Cancer Center, University of North Carolina at Chapel Hill, Chapel Hill, NC 27599, USA

^dDepartment of Chemistry, Westminster College, New Wilmington, PA 16172

^eUNC/NCSU Joint Department of Biomedical Engineering, Chapel Hill, NC 27599, USA

^fDepartment of Pharmaceutics, School of Pharmacy, China Medical University, Shenyang, Liaoning, 110122, P.R. China

^gInstitute of Medicinal Plant Development, Chinese Academy of Medical Sciences & Peking Union Medical College, Beijing 100193, P.R. China

Abstract

Chemoradiotherapy (CRT) with paclitaxel (PTX) and cisplatin (CP) is part of the standard of care for patients with locally advanced non-small cell lung cancer (NSCLC). Despite the high treatment intensity, many patients still develop local recurrence after treatment. Thus, there is a strong need to further improve CRT for lung cancer. One strategy is to co-deliver cytotoxic chemotherapy agents using biocompatible nanoparticles (NPs) which can limit off-target tissue toxicity and improve therapeutic efficacy. Herein, we report the development of dual-drug loaded nanoformulations that improve the efficacy of CRT for NSCLC by co-encapsulation of cisplatin (CP) and PTX in PLGA-PEG NPs. Mice bearing NSCLC xenografts given the dual-drug loaded NPs during CRT showed greater inhibition of tumor growth than free drug combinations or combinations of single-drug loaded NPs. These results indicate that using a NP co-delivery strategy for this common CRT regimen may improve clinical responses in NSCLC patients.

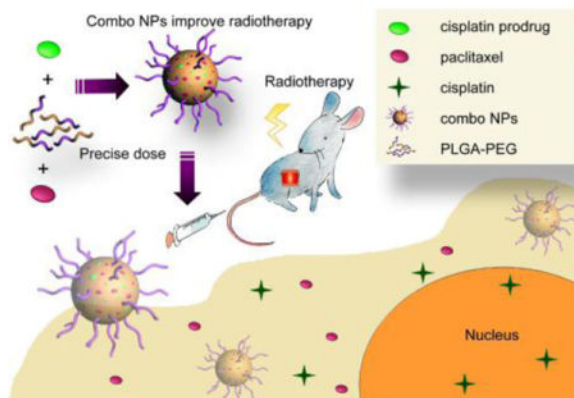
TOC image

*Corresponding author. zawang@med.unc.edu Phone: 1-(919)-966-7700.

†These authors contributed equally to this work.

Electronic Supplementary Information (ESI) available: [details of any supplementary information available should be included here]

Nanoparticles co-loaded with paclitaxel and cisplatin potentially enhance chemoradiotherapy in non-small cell lung cancer models versus the conventional free drug combination by delivering a precise therapeutic ratio.



Introduction

Lung cancer is the leading cause of cancer mortality.¹ Early manifestations of the disease can be treated via surgery. However, many NSCLC patients have locally advanced disease.² In these cases, CRT, typically consisting of CP (or similar carboplatin), PTX, and thoracic radiation, is the standard treatment.^{3–5} Despite extensive clinical trials optimizing this CRT regimen, there are still high rates of local failure. Furthermore, the enhanced potency of this CRT combination leads to increases in side effects and off-target toxicity. Hence, there has been strong interest in further improving CRT for NSCLC.

As a possible solution, NP delivery of chemotherapeutic combinations has proven a viable strategy to both improve responses and reduce side effects. NPs can preferentially accumulate drugs within tumors and limit off-target site exposure. Furthermore, carefully engineered, dual-drug loaded NPs can deliver chemotherapies in a precise therapeutic ratio to take advantage of synergistic effects or overcome multi-drug resistance.^{6–8} For example, liposomal co-formulations of cytarabine and daunorubicin have greatly improved clinical efficacy and reduced side effects in patients with acute myeloid leukemia.^{9,10} Other preclinical, NP based drug combinations have shown similar improvements in efficacy and toxicity profiles versus free drugs.^{11–17}

Given these advantages, we investigated NP co-delivery of the standard CP and PTX treatment regimen to improve CRT in murine models of NSCLC (Figure 1). We utilized FDA-approved poly(lactic acid-*co*-glycolic acid)-poly(ethylene glycol) (PLGA-PEG) NPs as our drug delivery system due to their excellent biocompatibility, high drug loading, ease of formulation, and potential for rapid clinical translation.^{18,19} PTX loads easily into the hydrophobic PLGA core, but hydrophilic CP shows poor encapsulation and low loading wt % within this environment. Therefore, to improve CP's co-loading with PTX in the NP's hydrophobic core, we employed a fatty acid modified CP prodrug (CPP) that has increased hydrophobicity (Figure S1).²⁰ This NP co-delivery strategy showed superior reductions in NSCLC tumor growth rates versus conventional CRT.

Results

NP Drug Loading and Release Kinetics

Biocompatible PLGA-PEG NPs encapsulate hydrophobic drugs, especially taxanes, within their hydrophobic PLGA core.^{18,19,21,22} However, hydrophilic CP shows poor loading efficiency within this hydrophobic environment. Therefore, we utilized a caprylic acid (C₈ fatty acid) modified Pt(IV) prodrug strategy that increases CP's loading into PLGA-PEG NPs. Upon release from the NP, the CPP's (Pt^{IV}) reduction by intracellular reductants (e.g., glutathione, ascorbate) produces active, square planar CP (Pt^{II}) (Figure S1).^{20,23–27}

NPs were loaded with drugs during nanoprecipitation. We analyzed the loading wt% and encapsulation efficiency (%EE) of both CPP and PTX in single-drug loaded PLGA-PEG NPs at a range of feeding ratios (FR, 2 – 16 wt%) (Figure S2, Table S1). As expected, the hydrophobic CPP loaded efficiently with a maximum loading wt% reaching $1.9 \pm 0.1\%$ (16 %EE) at 10 wt% FR (Figure S2a). Increasing the initial FR past 10 wt% failed to further increase the amount of loaded CPP. %EE expectantly fell from a maximum of $33.4 \pm 0.9\%$ (at 2% FR) with increasing FRs. The PTX loading wt% reached maximum levels ($2.8 \pm 0.1\%$) at a FR of 12 wt%, and its %EE reached a maximum of $39.4 \pm 1.0\%$ (at 2% FR) (Figures S2b).

We next investigated the effects that co-encapsulation in a single nanoformulation had on each drugs' loading (Figure 2, Table S2). Since CPP loaded maximally at a FR of 10 wt%, the CPP FR was held at this level, while the PTX dose varied. Maximum PTX loading (8 wt % FR) was approximately the same in the presence of CPP ($2.3 \pm 0.2\%$) versus when loaded alone ($2.4 \pm 0.2\%$). Similarly, CPP loading decreased only slightly ($1.9 \pm 0.1\%$ to $1.7 \pm 0.1\%$) with increased PTX FRs. Co-encapsulation and increasing PTX concentration also had a limited effect on particle size, polydispersity, and zeta potential (Figure 2c, Figure S3). This limited interdependence of loading allowed for facile production of uniform NPs at a range of CPP:PTX ratios (3:1 to 1:3).

We also determined whether co-loading both drugs into the NP would affect release kinetics under physiological sink conditions (Figure S4).²⁸ In both single-drug and dual-drug loaded NPs, the encapsulated PTX always released faster than CPP. Moreover, co-loading drugs into a single nanoformulation slowed the release rates for both CPP ($t_{1/2}$ - 6.8 ± 0.1 h for single-drug loaded to 9.2 ± 0.3 h for dual-drug loaded) and PTX ($t_{1/2}$ - 3.6 ± 0.2 h for single-drug to 5.3 ± 0.1 h for dual-drug).

Comparison of NP *In Vitro* Cytotoxicity

We selected three representative NSCLC cell lines (344SQ, H460, and A549) and one small-cell lung cancer (SCLC) cell line (H69AR) to examine differences in potency between various nanoformulations (Figure 3a, Table S3). Across all cell types, the single-drug loaded CPP NPs greatly increased drug potency versus free CP (5 [A549] to 100 [H460] fold IC₅₀ enhancements). However, this trend did not hold for single-drug loaded PTX NPs as their IC₅₀ values slightly increased upon encapsulation (75% IC₅₀ increase [A549] to 6-fold IC₅₀ reduction [344SQ]).

We analyzed the IC₅₀ concentrations of PTX:CPP combinations at ratios of 3:1, 1:1, and 1:3. For all cell lines, a drug ratio of 1:1 produced the greatest response. In the free drug arms, the 1:1 combination increased potencies versus PTX (the most potent, small molecule monotherapy) by 2.3 (H69AR) to 13.4 (344SQ) fold. Likewise, 1:1 mixtures of single-drug loaded NPs decreased required drug concentrations versus CPP NPs (the most potent NP monotherapy) by 2.2 (H69AR) to 10.9 (H460) fold. These IC₅₀ enhancements were nearly identical for the 1:1 dual-drug loaded NPs compared to the CPP NPs alone (2.9 [H69AR] to 9.6 [H460] fold). However, at all ratios tested, there were no significant differences in the potency between mixtures of single-drug loaded NPs or the dual-drug loaded formulations. Since the PTX:CPP ratio of 1:1 generally produced the greatest cytotoxicity, we used this formulation in all further investigations.

In addition to chemotherapy, oncologists employ concurrent radiotherapy (XRT) to treat NSCLC^{3–5}. Therefore, we investigated the ability of our NPs (1:1 PTX:CPP ratio) to radiosensitize two NSCLC cell lines (344SQ and H460) using the clonogenic survival assay (Figure 3b).¹⁵ Cells were treated with PTX:CPP formulations, exposed to increasing doses of radiation, and then plated to monitor colony formation. As expected, cells treated with any drug combination responded better to radiation treatment than the control arm (PBS). Both NPs (mixtures of single-drug loaded or dual-drug loaded) further reduced cell survival than the free drug combination at higher radiation doses (> 4 Gy). However, minimal difference existed between simply treating cells with a mixture of single-drug loaded NPs or dual-drug loaded NPs.

***In Vivo* Efficacy**

We probed the *in vivo* CRT efficacy of our NPs against murine NSCLC xenograft models (Figure 4). Mice were treated with free drugs, mixed single-drug loaded NPs, or dual-drug loaded NPs at the same sub-therapeutic dose (50% MTD) to enable monitoring of tumor growth rate differences. The two NP arms outperformed the standard free drug, CRT combination by producing a statistically significant reduction in tumor growth. Furthermore, the dual-drug loaded NPs blunted tumor growth better than administration of a combination of single-drug loaded NPs in the 344SQ model ($p < 0.05$) and to a lesser, not statistically significant degree in the H460 model ($p = 0.08$).

We analyzed tumor histology for cleaved caspase 3, a prognostic marker for early-stage apoptosis, in each treatment arm (Figure 5). Mice treated with NPs showed a greater degree of apoptosis than mice given CRT in free drug form. Moreover, the dual-drug loaded NPs produced apoptosis to a greater degree than using a mixture of single-drug loaded NPs ($p < 0.01$).

We also analyzed tumor sections for the enhanced delivery of CP and formation of CP-DNA adducts via immunofluorescence (Figure S5–S6). The sections from NP treatment arms showed a significant increase in CP-DNA adduct formation versus the free drug combination corresponding to an increased delivery of CP. The appearance of apoptotic features in the tumor histology also qualitatively indicates enhanced killing of tumor cells using this regimen (Figure S7).

Aside from the tumor, PLGA-PEG NPs tend to biodistribute to the liver and kidneys.^{15,29–32} Therefore, we examined if our nanoformulations caused undue toxicity to these off-target organs. Although the combination had higher treatment potency *in vivo*, nephrotoxicity and hepatotoxicity remained low as indicated by normal creatine (Crea), blood urea nitrogen (BUN), alanine aminotransferase (ALT), and aspartate aminotransferase (AST) levels in the blood (Table S4). However, the body weight of the animals did expectantly decrease post XRT but recovered gradually to baseline levels within several days (Figure S8).

Discussion

CRT for locally advanced NSCLC uses a combination of platinum and taxane derivatives.^{3–5} This combination works synergistically to radiosensitize cancer cells. However, research advances in this field have largely been limited to determining optimal dosing regimens and protocols (e.g., radiation & chemotherapy order, fractionation, etc.). Moreover, this chemotherapy and XRT combination can be highly toxic to the large volumes of healthy tissue exposed during treatment.

NP co-delivery of chemotherapy combinations has several important advantages that can improve clinical responses and address these challenges.^{6–8} First, PLGA-PEG NPs improve the solubility and the pharmacokinetic profile of a wide range of small-molecule drugs.^{28,30,32,33} Moreover, they can be designed to accommodate several drugs, even with vastly different solubilities and stabilities, into a single nanoformulation. This allows for the delivery of precise ratios of drugs that can induce combination synergy and overcome multi-drug resistance mechanisms.^{9,10,34–36} Finally, NPs can preferentially deliver drugs to tumor beds and avoid toxicities associated with whole body exposure. Due to these reasons, we sought to develop a single nanoformulation that delivers an optimum dose of PTX and CP together for improved CRT (Figure 1).

We chose PLGA-PEG NPs as our delivery system due to their ease of encapsulation of a wide range of drugs during nanoprecipitation, excellent biocompatibility, and potential for rapid clinical translation. The hydrophobic PLGA core is an especially excellent carrier for taxanes. However, hydrophilic CP loads poorly into these NPs' cores.

To circumvent this, we employed a prodrug strategy (CPP) that utilizes fatty acid modified CP to increase the drug's hydrophobicity and encapsulation into the PLGA core.²⁰ Several previous studies have shown that most CPPs undergo conversion to active, square planar CP (Pt^{II}) upon reduction.^{20,23–26} Conveniently, cancer cells often have substantially elevated levels of biological reductants, especially glutathione³⁷, that can rapidly convert CPPs into active CP.^{27,38–41} CPP conversion to CP tends to follow first-order kinetics with respect to the concentration of these reducing agents. Therefore, CPPs provide an ideal strategy to enable delivery of active CP to tumor cells via PLGA-PEG NPs.

NP Drug Loading and Release Kinetics

The octanoic acid modified CPP and PTX co-precipitated efficiently within PLGA NPs and did not significantly affect each other's loading (Figure 2, Figure S2, Table S1–S2). This allowed for the facile synthesis of nanoformulations at a wide range of PTX:CPP ratios (3:1

to 1:3). Moreover, loading of both drugs into NPs did not substantially affect the vehicle's properties (Figure 2, Figure S3). This broad loading adaptability of the PLGA-PEG system may allow for the delivery and screening of potentially synergistic drug ratios to achieve maximum therapeutic effect.

In contrast to drug loading and particle properties, the co-loaded drugs did slightly affect each other's release rates (Figure S4). This is possibly due to increased interactions between the hydrophobic molecules within the PLGA core leading to greater retention. Provided the NP remains in circulation, this slower release profile could provide advantages in increasing the drugs' circulation time. However, co-encapsulation only increases drug retention half-life by a few hours, which makes ascertaining the full effects of this slower release difficult.

Comparison of NP *In Vitro* Cytotoxicity

Loading of the CPP into NPs substantially increased CP's observed cytotoxicity up to 100 fold versus the free drug (Figure 3, Table S3). This likely stems from improved delivery of CP into cells either via an increase in CPP passive cell permeability or NP phagocytosis and endosomolysis. Both effects circumvent common NSCLC resistance mechanisms, such as low expression of copper transporter 1, that block CP uptake.⁴² Encapsulation of PTX in NPs did not increase its potency, indicating PTX cellular permeation remains largely unaffected.

As expected, combining both drugs lowered the cumulative IC₅₀, likely due to the drugs differing mechanisms of action. CP induces DNA double strand breaks, while PTX promotes microtubule stabilization. Together, these drugs have at least an additive effect and can overcome drug resistance. Encapsulation of the drug combination in NPs further enhanced the cytotoxic effects, likely due to the increased potency and delivery of the CP component. However, delivering the combination either by mixing single-drug loaded NPs or co-encapsulation in a single NP showed no differences in cytotoxicity. This suggests no advantage in an *in vitro* setting to co-encapsulation. As there are no barriers to delivery of a specific drug ratio or differences in pharmacokinetics in a culture flask, the advantages of co-encapsulation, such as equal extravasation of a specific drug ratio into the tumor bed, would not be evident unless applied *in vivo*.

In Vivo Efficacy

The dual-drug loaded NPs (1:1 PTX:CPP) outperformed a mixture of single-drug loaded NPs *in vivo* for both 344SQ ($p < 0.05$) and H460 ($p = 0.08$) (Figure 4). Even more promising, the combination loaded NPs greatly retarded tumor growth rates compared to the free drug combination with XRT ($p = 0.01$ for both cell lines). It should be noted that the observed rapid growth rates of these tumors in all treatment arms stem from their high degree of aggressiveness and the sub-therapeutic dose administered to the animals (~50% MTD). Histologic analysis of tumor caspase 3 activity reciprocated these results with the combination NPs inducing the greatest early stage apoptosis (Figure 5).

Compared to the dual-drug loaded NPs, both the free drug combination and mixtures of single-drug loaded NPs likely do not expose the tumors to both drugs in the right ratio which leads to differences in efficacy. Indeed, the delivery of the specific 1:1 PTX:CPP drug

combination via a single nanoformulation was likely the causative factor in the increased apoptosis. The different physiochemical and pharmacokinetic properties of free CP and PTX likely shift both the dose and ratio of drug that eventually reaches the tumor when compared to dual-drug loaded NPs. At least part of this effect for CP is evident in the substantially increased CP-DNA adduct formation seen in tumors treated with dual-drug loaded NPs (Figure S5–S6). However, the discrepancy in efficacy between mixed single-drug loaded and dual-drug loaded NPs is not abundantly clear.

Comparison of the single-drug loaded NP properties provides a few possible explanations (Figure 2). First, the PTX NPs skewed smaller than the CPP NPs. Since size affects extravasation, this could cause the unequal tumor accumulation of one NP versus the other and shift the ratio of drug dose.²⁹ Second, the increased drug retention within the dual-drug loaded NPs may allow more of the drug to be delivered to the target site instead of escaping prior to NP permeation into the tumor.²⁸ Regardless, a full examination of the causative factors for the increased efficacy was outside the scope of this study, but ongoing work within the lab seeks to fully address possible mechanisms.

Conclusions

Co-encapsulation of CP and PTX in a single nanoformulation increases CRT's efficacy against NSCLC. This improved efficacy likely arises from enhanced dosing of the tumor with increased concentrations and precise ratios of drug compared to the free small molecules. The incorporation of biocompatible and easily synthesized PLGA-PEG NPs in this CRT regimen makes this system capable of rapid adaptation as a clinical tool. Therefore, we hope this research lays the ground work for further investigations on these formulations in NSCLC treatment.

Experimental

Additional experimental details on the materials used, cell culture techniques, tumor section staining and synthesis of prodrug precursors are provided in the Supplementary Information.

Preparation of single/dual-drug loaded PLGA-PEG NPs

PTX and/or CPP-loaded loaded PLGA-PEG NPs with different molar ratios were prepared via nanoprecipitation. PLGA-PEG (5 mg) and drugs at varying feeding ratios (w/w% to polymer, FR) were dissolved in acetonitrile (200 μ L). A 1:1 molar ratio of PTX:CPP was generated in dual-drug loaded NPs using a FR of 8 wt% PTX and 10 wt% CPP. Single-drug loaded NPs used *in vivo* were generated with these same FRs. The organic solution was then added dropwise to deionized water (4 mL) under constant stirring. The NPs were purified by filter centrifugation using an Amicron Ultra-4 filter (MWCO- 30 kDa) at 1000 \times g for 15 min (Millipore, Billerica, MA, USA). The PLGA-PEG NPs were washed 3 times with deionized water) then suspended in PBS.

Drug-loading determination

The amount of loaded CPP and PTX was measured using a Shimadzu SPD-M20A high-performance liquid chromatography (HPLC) instrument equipped with a diode array

detector and a reverse-phase GP-C₁₈ column (Sepax Technology Inc., Newark, DE, USA). NPs (10 μ L) were mixed with acetonitrile (50 μ L) and left overnight at 5 °C to dissolve the NP and drugs. Drugs were eluted using a binary solvent system (A:B, A- H₂O, B- CH₃CN, flow rate- 0.25 mL/min) that linearly increased from 0% to 100% B over 20 min (0–20 min), held at 100% B for an additional 5 min (20–25 min), then reduced to 50% B for the final 5 min (25–30 min). Drug elution was monitored at 227 nm for PTX and 245 nm for CPP. Retention times were: PTX- 11.9 min and CPP- 12.9 min. Drug concentrations were determined using area under the curve integration compared with drug standard curves. The limit of detection was estimated to be ~1 μ M for CP.

In Vitro Release of CPPs and PTX from PLGA-PEG NPs

In vitro drug-release profiles were recorded under physiological sink conditions.²⁸ NP solutions (2.2mg/mL, 500 μ L) were loaded into Slide-A-Lyzer MINI dialysis microtubes (20 kDa MWCO, Pierce, Rockford, IL, USA) and dialyzed against a large excess of PBS (1 L) stirring at 37 °C. At the indicated times, 10 μ L of residual NP test solution was removed from the microdialysis tube and dissolved in acetonitrile (60 μ L). The remaining chemotherapy concentrations were determined using the above HPLC method.

In Vitro Cytotoxicity of PLGA-PEG NPs

H460, 344SQ, A549 (5,000 cells/well), and H69AR (10,000 cells/well) were plated in a 96-well plate and incubated overnight. Cells were then dosed with different drug formulations at varying doses (10^{-9} – 10^{-5} M) in RPMI-1640 media. After 72 h incubation, cell viabilities were determined using a 3-(4,5-dimethylthiazol-2-yl)-5-(3-carboxymethoxyphenyl)-2-(4-sulfophenyl)-2H-tetrazolium (MTS) cell viability assay (Promega). The absorbance at 490 nm was recorded using a 96-well plate reader (Infinite 200 Pro, Tecan i-control) to determine response. The IC₅₀ values were calculated by fitting the dose-dependent cell viabilities to a four-parameter logistic model using MasterPlex 2010 software pack (MiraiBio Group, Hitachi Solutions America, Ltd.).

Clonogenic survival assay.¹⁵

Cells (10^6) were seeded in a 75 cm² flask overnight before treatment. Cells were treated with the predetermined therapeutic dose (i.e., IC₅₀) of small-molecule or encapsulated drugs for 3–4 h and washed three times with cold PBS. Cells were then trypsinized and re-suspended in cold complete culture medium. Cell mixtures with densities ranging from 100 to 10,000 cells/mL were transferred to 6-well plates (2 mL/well). After 3–4 h, cells were irradiated with varying radiation doses (0, 2, 4, 6, or 8 Gy) from an X-RAD 320 (Precision X-ray) machine operating at 320 kVp and 12.5 mA. Fourteen days after irradiation, cell clones were fixed with paraformaldehyde (4 v/v%) and stained with crystal violet. Colonies containing 30 cells or more were counted, and surviving fractions were determined for both lines. The surviving fraction (SF) was calculated from the plating efficiency (PE) according to the following equations:

$$PE = (\# \text{colonies formed} / \# \text{cells plated}) \times 100\%$$

$$SF = \frac{\# \text{formed after treatment}}{(\# \text{cells seeded} \times PE)}.$$

The best-fit line for survival fraction was plotted on a log scale versus the radiation dose (D) and fit with the following linear-quadratic formula:

$$SF = e^{-\alpha D - \beta D^2}$$

where α is the linear parameter and β is the quadratic parameter.

In Vivo Anticancer efficacy of PLGA-PEG NPs

A murine, lung cancer xenograft model was generated by s.c. injection of 1×10^6 344SQ or H460 cells (100 μ L of 1×10^7 cells/mL, 50% v/v Matrigel®) into the left flank of female, athymic, nude mice. Tumors were allowed to grow to a volume 150–200 mm³ before initiating treatment. Mice were divided into six groups (5–6 mice per group) and treated once on day 0 via tail vein injection with either PBS (200 μ L), free CP (2.3 mg/kg) and PTX (5.0 mg/kg) formulated in cremophor EL, mixtures of single-drug loaded CPP NPs (3.9 mg/kg) and PTX NPs (5.0 mg/kg), and dual-drug loaded NPs with CPP (3.9 mg/kg) and PTX (5.0 mg/kg) NPs. Mice in CRT groups received 3×5 Gy X-ray irradiation 3 h, 24 h and 48 h after i.v. administration of chemotherapeutic agents using a Precision X-RAD 320 (Precision X-Ray, Inc) machine operating at 320 kVp and 12.5 mA. The dose rate at a source-subject distance of 70 cm was 0.5 Gy min⁻¹. Mice upper bodies were lead-shielded to protect most organs. Body weight and tumor volume were monitored every 2 days. The tumor volume was calculated using: $(L \times W^2)/2$, with W being smaller than L. Mice were sacrificed when tumor dimensions reached > 2 cm in one direction.

Immunofluorescent Staining for Active Caspase 3 and CP-DNA Adducts

Tumors were collected 2 days post treatment from the 344SQ model, fixed in neutral buffered formalin (4% v/v) at 4 °C for 24 h, then ethanol (70% v/v) at 4 °C for another 24 h. The tumor sections were de-paraffinized, antigen recovered, blocked with BSA (1% w/v), incubated overnight with a 1:400 dilution of cleaved caspase-3 (Asp175) antibodies (Cell Signaling Technology, MA), and then stained with Alexa Fluor® 594 Goat Anti-Rabbit IgG (1:2000, Life Technology, CA). For CP-DNA adduct formation, sections were incubated overnight with a 1:300 dilution of anti-CP-DNA antibody (CP9/19, Abcam, MA). The sections were counter-stained with VECTASHIELD mounting media containing DAPI (Vector Laboratories, Burlingame, CA). Tumor sections were imaged using an Olympus IX 81 inverted wide-field light microscope in the Microscopy Services Laboratory at the UNC Medical School.

Statistical analysis

All experiments were performed three times (n=3) and expressed as mean \pm SD for in vitro or mean \pm SEM for in vivo studies. Statistical differences were determined using two-tailed Student's t-test. The significance level was taken as 95% (P<0.05).

Supplementary Material

Refer to Web version on PubMed Central for supplementary material.

Acknowledgments

This work was supported by National Institutes of Health/National Cancer Institute (R01CA178748-01, R21 CA182322, and U54CA198999 for Carolina Center of Cancer Nanotechnology Excellence (CCNE)-Nano Approaches to Modulate Host Cell Response for Cancer Therapy). Jing Tian is supported by the Natural Science Foundation of Tianjin (Grant No. 15JCYBJC21100) and the Science & Technology Development Fund of Tianjin Education Commission for Higher Education (No. 20110511). Zachary Rodgers is supported by the Carolina Cancer Nanotechnology T32 Training Program (C-CNTP, NIH- 1T32CA196589).

References

1. Torre, LA., Siegel, RL., Jemal, A. Lung Cancer and Personalized Medicine: Current Knowledge and Therapies. Ahmad, A., Gadgeel, S., editors. Springer International Publishing; Cham: 2016. p. 1-19.
2. Goldstraw P, Ball D, Jett JR, Le Chevalier T, Lim E, Nicholson AG, Shepherd FA. Lancet. 2011; 378:1727–1740. [PubMed: 21565398]
3. Johnson DH, Schiller JH, Bunn PA. J Clin Oncol. 2014; 32:973–982. [PubMed: 24567433]
4. Salama JK, Vokes EE. J Clin Oncol. 2013; 31:1029–1038. [PubMed: 23401449]
5. Vokes EE, Herndon JE, Kelley MJ, Cicchetti MG, Ramnath N, Neill H, Atkins JN, Watson DM, Akerley W, Green MR. J Clin Oncol. 2007; 25:1698–1704. [PubMed: 17404369]
6. Ma L, Kohli M, Smith A. ACS Nano. 2013; 7:9518–9525. [PubMed: 24274814]
7. Hu CMJ, Zhang L. Biochem Pharmacol. 2012; 83:1104–1111. [PubMed: 22285912]
8. Greco F, Vicent MJ. Adv Drug Deliv Rev. 2009; 61:1203–1213. [PubMed: 19699247]
9. Raut L. South Asian J Cancer. 2015; 4:38. [PubMed: 25839020]
10. Lancet JE, Cortes JE, Hogge DE, Tallman MS, Kovacovics TJ, Damon LE, Komrokji R, Solomon SR, Kolitz JE, Cooper M, Yeager AM, Louie AC, Feldman EJ. Blood. 2014; 123:3239–3246. [PubMed: 24687088]
11. Shiao Y, Chiu H, Wu P, Huang Y. ACS Appl Mater Interfaces. 2014; 6:21832–21841. [PubMed: 24949657]
12. Kolishetti N, Dhar S, Valencia PM, Lin LQ, Karnik R, Lippard SJ, Langer R, Farokhzad OC. Proc Natl Acad Sci U S A. 2010; 107:17939–44. [PubMed: 20921363]
13. Miao L, Guo S, Zhang J, Kim WY, Huang L. Adv Funct Mater. 2014; 24:6601–6611. [PubMed: 25395922]
14. Liao L, Liu J, Dreaden EC, Morton SW, Shopsowitz KE, Hammond PT, Johnson JA. J Am Chem Soc. 2014; 136:5896–5899. [PubMed: 24724706]
15. Au KM, Min Y, Tian X, Zhang L, Perello V, Caster JM, Wang AZ. ACS Nano. 2015; 9:8976–8996. [PubMed: 26267360]
16. Tian J, Min Y, Rodgers Z, Wan X, Qiu H, Mi Y, Tian X, Wagner KT, Caster JM, Qi Y, Roche K, Zhang T, Cheng J, Wang AZ. Nanomedicine Nanotechnology, Biol Med. 2017; 13:1301–1307.
17. Guo S, Lin CM, Xu Z, Miao L, Wang Y, Huang L. ACS Nano. 2014; 8:4996–5009. [PubMed: 24720540]
18. Danhier F, Ansorena E, Silva JM, Coco R, Le Breton A, Pr at V. J Control Release. 2012; 161:505–522. [PubMed: 22353619]
19. Pavot V, Berthet M, R ess equier J, Legaz S, Handk e N, Gilbert SC, Paul S, Verrier B. Nanomedicine. 2014; 9:2703–2718. [PubMed: 25529572]
20. Johnstone TC, Lippard SJ. Inorg Chem. 2013; 52:9915–9920. [PubMed: 23859129]
21. Kim TY. Clin Cancer Res. 2004; 10:3708–3716. [PubMed: 15173077]
22. Hrkach J, Von Hoff D, Ali MM, Andrianova E, Auer J, Campbell T, De Witt D, Figa M, Figueiredo M, Horhota A, Low S, McDonnell K, Peeke E, Retnarajan B, Sabnis A, Schnipper E, Song JJ, Song YH, Summa J, Tompsett D, Troiano G, Van Geen Hoven T, Wright J, LoRusso P, Kantoff

- PW, Bander NH, Sweeney C, Farokhzad OC, Langer R, Zale S. *Sci Transl Med*. 2012; 4:128ra39–128ra39.
23. Hall MD, Dillon CT, Zhang M, Beale P, Cai Z, Lai B, Stampfl APJ, Hambley TW. *J Biol Inorg Chem*. 2003; 8:726–732. [PubMed: 12884089]
24. Hall MD, Mellor HR, Callaghan R, Hambley TW. *J Med Chem*. 2007; 50:3403–3411. [PubMed: 17602547]
25. Kelland L. *Nat Rev Cancer*. 2007; 7:573–584. [PubMed: 17625587]
26. Dhar S, Kolishetti N, Lippard SJ, Farokhzad OC. *Proc Natl Acad Sci*. 2011; 108:1850–1855. [PubMed: 21233423]
27. Wexselblatt E, Gibson D. *J Inorg Biochem*. 2012; 117:220–229. [PubMed: 22877926]
28. Sethi M, Sukumar R, Karve S, Werner ME, Wang EC, Moore DT, Kowalczyk SR, Zhang L, Wang AZ. *Nanoscale*. 2014; 6:2321–7. [PubMed: 24418914]
29. Caster JM, Yu SK, Patel AN, Newman NJ, Lee ZJ, Warner SB, Wagner KT, Roche KC, Tian X, Min Y, Wang AZ. *Nanomedicine Nanotechnology Biol Med*.
30. Rafiei P, Haddadi A. *Int J Nanomedicine*. 2017; 12:935–947. [PubMed: 28184163]
31. Semete B, Booyens L, Kalombo L, Ramalapa B, Hayeshi R, Swai HS. *Int J Pharm*. 2012; 424:115–120. [PubMed: 22227605]
32. Li M, Panagi Z, Avgoustakis K, Reineke J. *Int J Nanomedicine*. 2012; 7:1345–1356. [PubMed: 22419876]
33. Rafiei P, Haddadi A. *Pharm Nanotechnol*. 2017; 5:3–23.
34. Lehár J, Krueger AS, Avery W, Heilbut AM, Johansen LM, Price ER, Rickles RJ, Short GF III, Staunton JE, Jin X, Lee MS, Zimmermann GR, Borisy AA. *Nat Biotechnol*. 2009; 27:864–864.
35. Tallarida RJ. *Genes Cancer*. 2011; 2:1003–1008. [PubMed: 22737266]
36. Jia J, Zhu F, Ma X, Cao ZW, Li YX, Chen YZ. *Nat Rev Drug Discov*. 2009; 8:111–28. [PubMed: 19180105]
37. Hong R, Han G, Fernández JM, Kim B, Forbes NS, Rotello VM. *J Am Chem Soc*. 2006; 128:1078–1079. [PubMed: 16433515]
38. Lemma K, Berglund J, Farrell N, Elding LI. *J Biol Inorg Chem*. 2000; 5:300–6. [PubMed: 10907740]
39. Kratochwil NA, Bednarski PJ. *Arch Pharm (Weinheim)*. 1999; 332:279–85. [PubMed: 10489538]
40. Kratochwil NA, Bednarski PJ. *J Cancer Res Clin Oncol*. 1999; 125:690–6. [PubMed: 10592102]
41. Zhu Z, Wang Z, Hao Y, Zhu C, Jiao Y, Chen H, Wang YM, Yan J, Guo Z, Wang X. *Chem Sci*. 2016; 7:2864–2869.
42. Min Y, Mao CQ, Chen S, Ma G, Wang J, Liu Y. *Angew Chemie Int Ed*. 2012; 51:6742–6747.

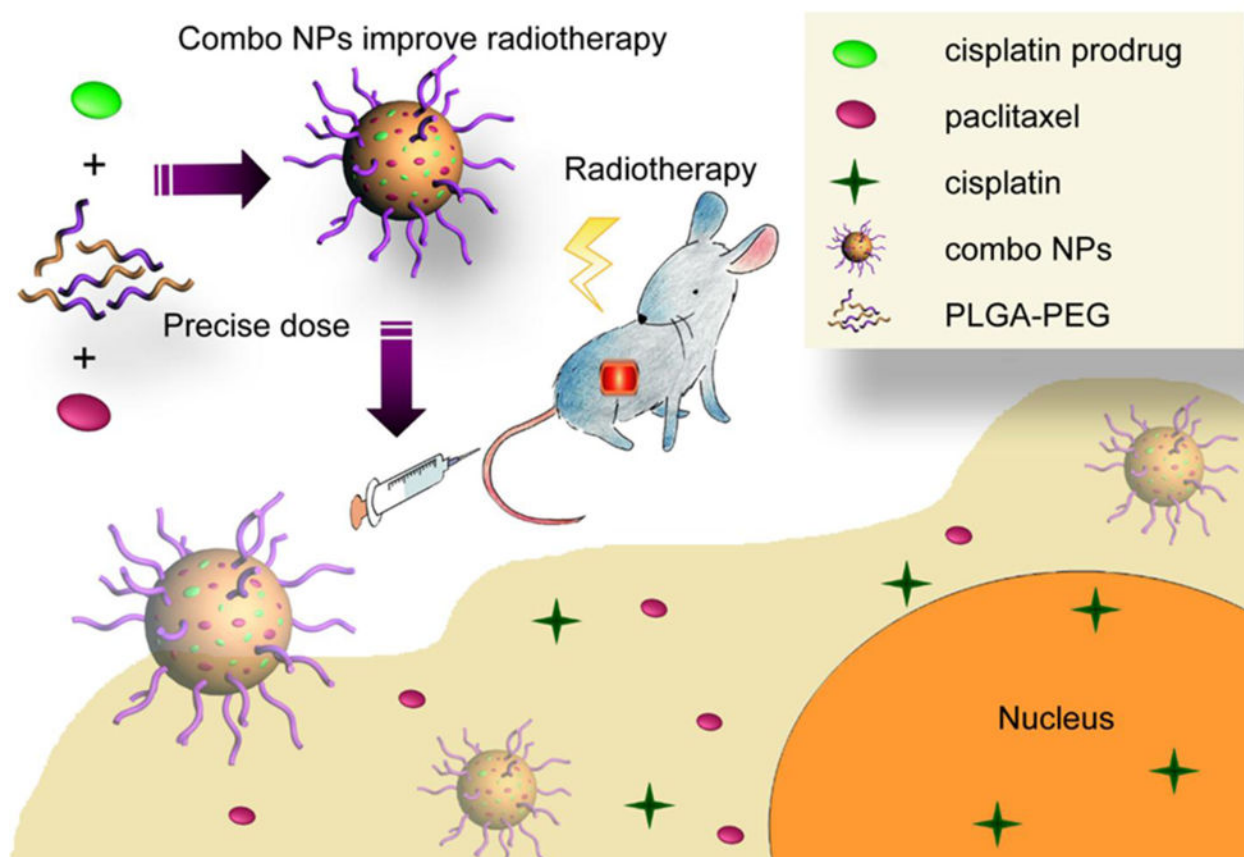


Figure 1.

Co-encapsulation of CPP and PTX in PLGA-PEG NPs provisions a precise dose of drug to the tumor and efficiently potentiates CRT.

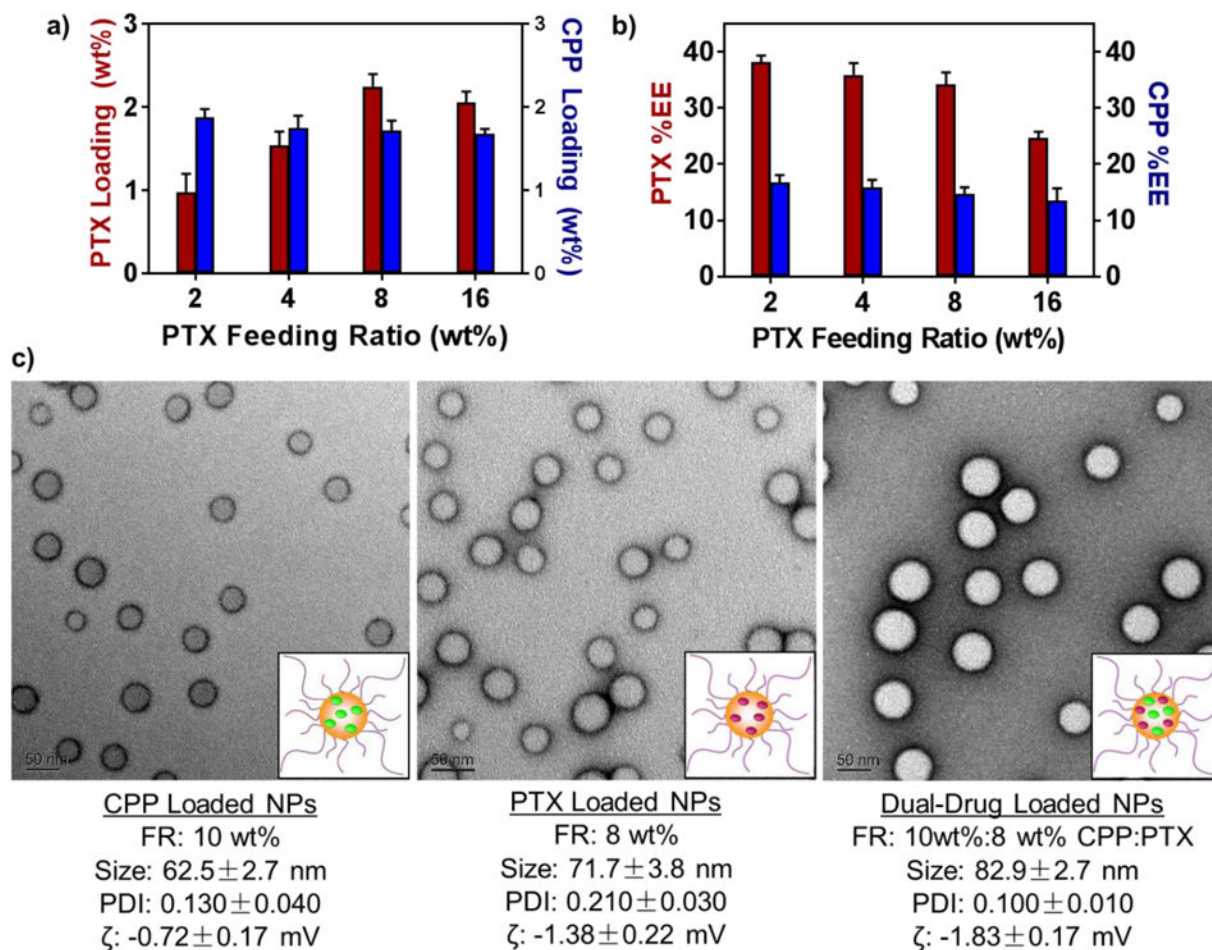


Figure 2.

a) Drug loading (wt%) and **b)** encapsulation efficiency (%EE) in dual-drug loaded NPs. The FR of CPP was held constant at 10 wt%, while the PTX %FR was varied (2 – 16 wt%). **c)** TEM images and characterization data for NPs used *in vivo*. The dual-drug loaded NPs contained a loaded PTX:CPP molar ratio of 1:1.

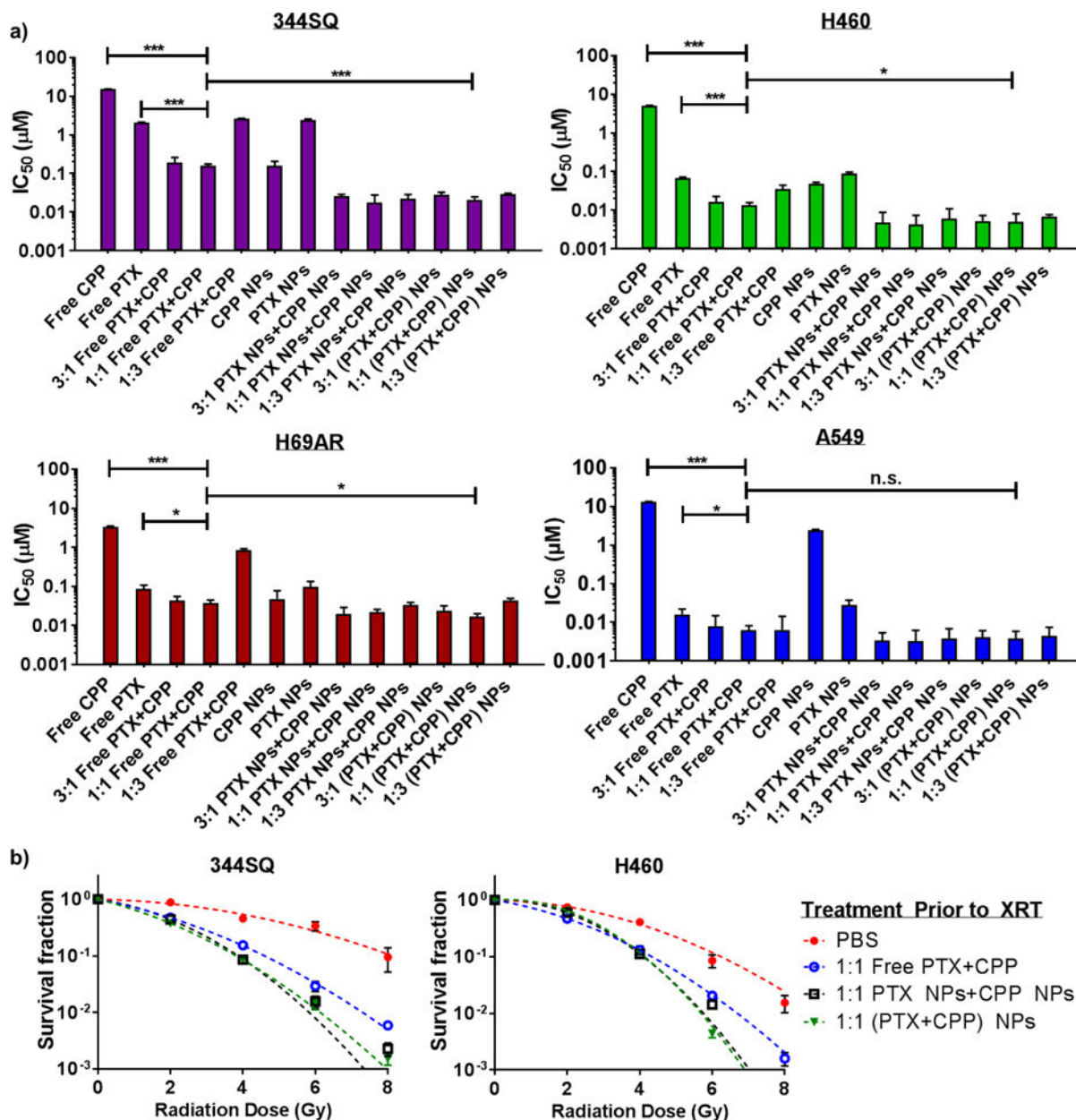


Figure 3.

a) *In vitro* cytotoxicities of free and encapsulated chemotherapeutics in non-small cell (H460, 344SQ, and A549) and small cell (H69AR) lung cancer cell lines. (* p < .05, ** p < .01, *** p < .001, n.s. = not significant). When a combination was used, a PTX:CPP ratio will be indicated at the beginning of each arm's label. *Free* indicates non-encapsulated drugs, *PTX NP + CPP NP* indicates a mixture of single-drug loaded NPs, and *(PTX+CPP) NPs* indicates dual-drug loaded NPs. **b)** *In vitro* radiosensitizing efficiencies of small-molecule and encapsulated drugs.

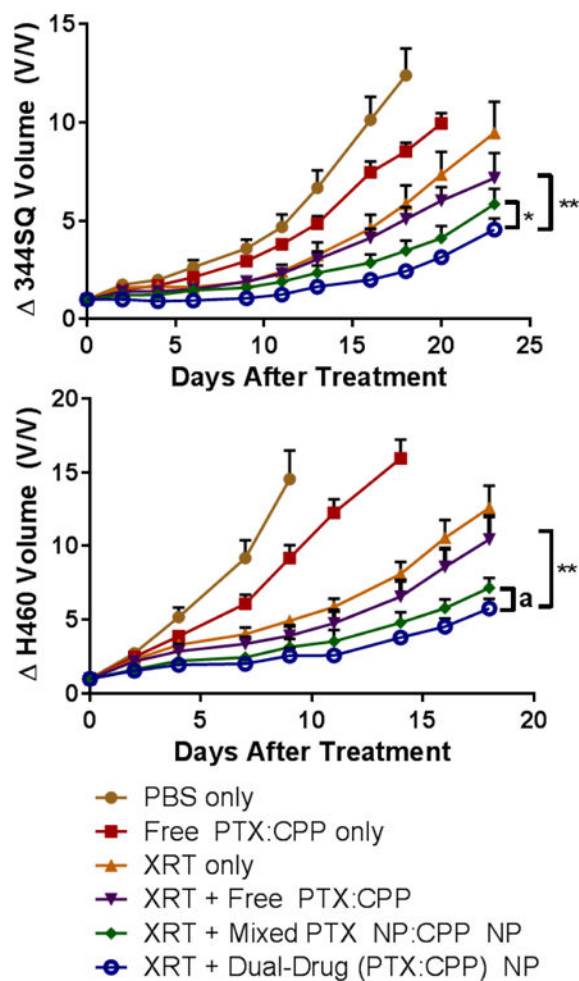


Figure 4. In vivo

CRT efficacy comparison between free drugs and NP formulations in **a)** 344SQ and **b)** H460 xenograft models. (* p < .05, ** p < .01, a = .08). Mice were administered chemotherapies (1:1 PTX:CPP molar ratio, 5 mg/kg PTX and 2.3 mg/kg CP or 3.9 mg/kg CPP) once on day 0. Mice receiving XRT were irradiated with 5 Gy at 3, 24, and 48 h (15 Gy total) post chemotherapy administration. The data are represented as the change in tumor volume after tumors become palpable.

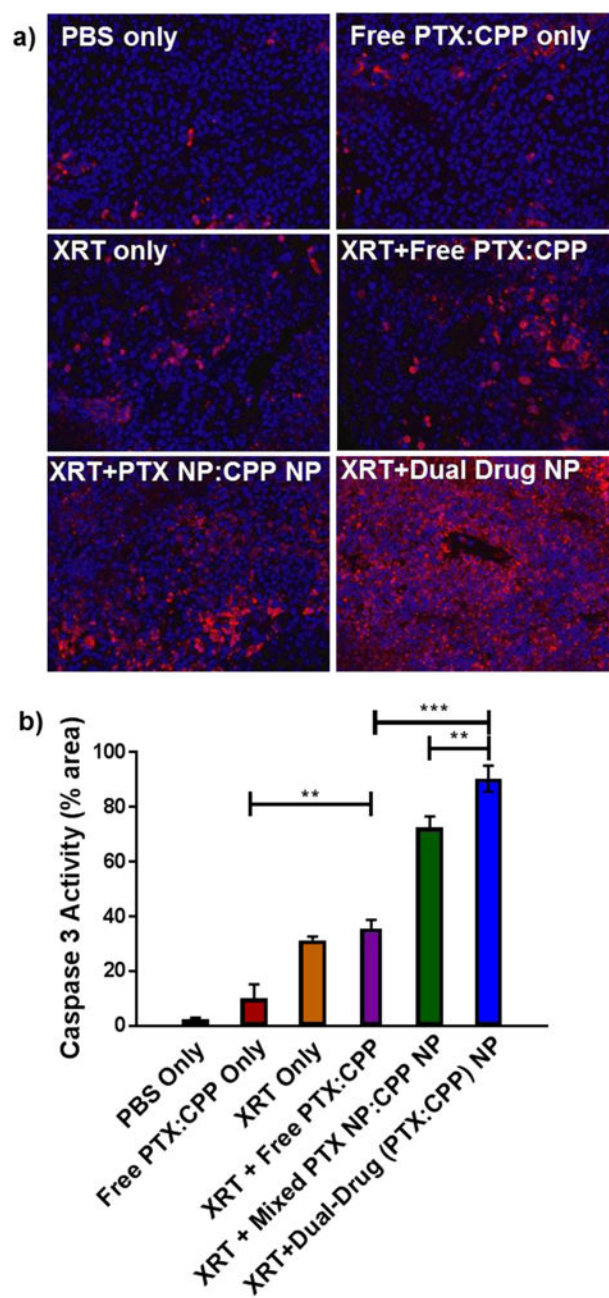


Figure 5.

a) Fluorescent microscopy images of caspase 3 (red) activation in H460 xenograft tumors after treatment. Nuclei were stained with Hoechst stain (blue) **b)** Quantified caspase 3 activity represented as a proportion of the total red fluorescence area. Elevated caspase 3 activity signifies apoptosis due to treatment (* $p < .05$, ** $p < .01$, *** $p < .001$, n.s. = not significant)